ESC European Society of Cardiology

Europace (2018) **20**, iii45–iii54
doi:10.1093/europace/euy234

ORIGINAL RESEARCH

Arrhythmia dynamics in computational models of the atria following virtual ablation of re-entrant drivers

Joe B. Hakim[1], Michael J. Murphy[1], Natalia A. Trayanova[1], and Patrick M. Boyle[1,2]*

[1]Institute for Computational Medicine and Department of Biomedical Engineering, Johns Hopkins University, 3400 N. Charles St, 208 Hackerman Hall, Baltimore, MD 21218, USA; and [2]Department of Bioengineering, University of Washington, N310H Foege, Box 355061, Seattle WA 98195-5061, USA

Received 11 September 2018; editorial decision 17 September 2018; accepted 18 September 2018

Aims Efforts to improve ablation success rates in persistent atrial fibrillation (AF) patients by targeting re-entrant driver (RD) sites have been hindered by weak mechanistic understanding regarding emergent RDs localization following initial fibrotic substrate modification. This study aimed to systematically assess arrhythmia dynamics after virtual ablation of RD sites in computational models.

Methods and results Simulations were conducted in 12 patient-specific atrial models reconstructed from pre-procedure late gadolinium-enhanced magnetic resonance imaging scans. In a previous study involving these same models, we comprehensively characterized pre-ablation RDs in simulations conducted with either 'average human AF'-based electrophysiology (i.e. EP_{avg}) or ±10% action potential duration or conduction velocity (i.e. EP_{var}). Re-entrant drivers seen under the EP_{avg} condition were virtually ablated and the AF initiation protocol was re-applied. Twenty-one emergent RDs were observed in 9/12 atrial models (1.75 ± 1.35 emergent RDs per model); these dynamically localized to boundary regions between fibrotic and non-fibrotic tissue. Most emergent RD locations (15/21, 71.4%) were within 0.1 cm of sites where RDs were seen pre-ablation in simulations under EP_{var} conditions. Importantly, this suggests that the level of uncertainty in our models' ability to predict patient-specific ablation targets can be substantially mitigated by running additional simulations that include virtual ablation of RDs. In 7/12 atrial models, at least one episode of macro-reentry around ablation lesion(s) was observed.

Conclusion Arrhythmia episodes after virtual RD ablation are perpetuated by both emergent RDs and by macro-reentrant circuits formed around lesions. Custom-tailoring of ablation procedures based on models should take steps to mitigate these sources of AF recurrence.

Keywords Atrial fibrillation • Fibrotic remodelling • Patient-specific computational models • Catheter ablation • Re-entry

Introduction

Atrial fibrillation (AF) is the most prevalent sustained cardiac arrhythmia, causing morbidity and mortality in 3–5 million individuals in the United States alone.[1] The severity of AF is exacerbated by its progressive nature. Each year, electrophysiological and fibrogenic remodelling of atrial tissue lead to the development of persistent AF (PsAF) in approximately 5% of AF patients,[2] resulting in prolonged arrhythmia episodes (≥7 days) and extremely limited treatment options.[3] Success rates for the standard-of-care treatment option, pulmonary vein isolation (PVI) via catheter ablation, are sub-optimal (∼50%) in patients with PsAF.[4] This is partly attributed to disease-related remodelling of the atria, which creates a substrate for the initiation and perpetuation of spiral waves [i.e. re-entrant drivers (RDs)] that promote fibrillatory activity.[5,6]

Despite promising preliminary results,[7,8] attempts to improve PsAF ablation success rates by ablating RD sites identified by intracardiac mapping [i.e. focal impulse and rotor mapping (FIRM)] have yet

* Corresponding author. Tel: +1 206 685 1392; fax: +1 206 685 3300. *E-mail address*: pmjboyle@uw.edu

What's new?

- Our computational simulations of atrial fibrillation induced after virtual ablation of an initial set of re-entrant drivers (RDs) indicate that post-ablation arrhythmias can be perpetuated by emergent RDs at new locations in the fibrotic substrate or by macro-reentrant circuits that form around lesions.
- Similar to pre-ablation RDs, emergent RDs dynamically localize to atrial regions at boundaries between fibrotic and non-fibrotic tissue.
- Emergent RDs observed in post-ablation simulations occurred in the same atrial regions where RDs were seen in pre-ablation simulations conducted under different electrophysiological conditions (±10% action potential duration, conduction velocity), suggesting that model uncertainty can be substantially mitigated by conducting virtual RD ablations to determine the optimal personalized set of ablation targets.

to show therapeutic benefit over PVI alone.[9] Modest success rates (~80%) have been reported for targeted ablation of RDs based on non-invasive electrocardiographic imaging (ECGI),[6] but long-term follow-up and multi-centre validation of this approach are lacking. Overall, no definitive approach has emerged for effective catheter ablation of the fibrotic substrate in PsAF. One explanation for the high rate of AF recurrence in patients who undergo treatment is the emergence of post-ablation RDs in the modified fibrotic substrate. There is a lack of mechanistic understanding of the dynamic localization of such emergent RDs in the substrate. An attempt to uncover these mechanisms has been made in simple computational models (i.e. two-dimensional sheets of simulated atrial tissue)[10] but never in realistic organ-scale models including detailed representations of atrial geometry and patient-specific patterns of structural remodelling.

We have recently developed an atrial modelling approach that has provided a valuable platform for understanding AF mechanisms and developing new treatment strategies including personalized ablation planning based on analysis of simulation results.[11–18] In these models, the personalized element is limited to information that can be extracted from non-invasive late gadolinium-enhanced magnetic resonance imaging (LGE-MRI) scans (i.e. patient-specific atrial geometry and the spatial distribution of fibrotic tissue) but cell- and tissue-scale electrophysiology are represented using an 'average human AF'-based model (i.e. EP_{avg}). This is because relevant patient-specific electrophysiological properties cannot be obtained non-invasively. Recently, we showed that this lack of electrophysiological personalization leads to a level of uncertainty in the locations of calculated AF ablation targets.[14] Specifically, RDs induced in atrial models with ±10% APD/CV variability (i.e. EP_{var}) were sometimes observed in locations that had never been observed in EP_{avg} simulations. Due to the lack of knowledge regarding post-ablation arrhythmia dynamics, it remains unclear whether virtual ablation of RDs originally observed under EP_{avg} conditions might be able to unmask emergent RD locations that were previously only seen under EP_{var} conditions in pre-ablation models.

Thus, the goal of this study is to systematically assess arrhythmia dynamics, and in particular, emergent RDs, in atrial models following virtual ablation of RDs identified pre-ablation. We hypothesize that if all RDs observed in a particular model under EP_{avg} conditions are virtually ablated and then AF initiation is attempted a second time, new AF episodes will be perpetuated by emergent RDs. We further hypothesize that the locations unmasked by this process will correspond to RD sites that were previously only seen under EP_{var} conditions in pre-ablation models.

Methods

Reconstruction of patient-specific atrial models

We used 12 patient-specific atrial models; these have been used in our earlier work.[14] As described previously,[12] these models were derived from LGE-MRI scans acquired for individuals with PsAF, which was defined as uninterrupted AF lasting longer than 7 days.[19] Detailed information about the atrial model reconstruction pipeline can be found in previous published work.[12–16] Briefly, regions of fibrotic and non-fibrotic myocardium were delineated using a validated algorithm based on image intensity ratio,[20] and fibre orientations were assigned using an image-based estimation approach.[12,21–24] We used this approach because no method currently exists that is capable of non-invasively measuring coupling anisotropy in the human heart. The resulting distributions of fibre orientations are qualitatively similar to those reported from *ex vivo* analysis of human atria.[25,26]

Modelling electrophysiology of the fibrotic atria

The approach used here to represent excitation propagation in fibrotic atrial tissue of PsAF patients is described in our earlier published articles.[12–16] All relevant cell- and tissue-scale parameters controlling myocyte membrane kinetics and conduction velocities within fibrotic and non-fibrotic regions were calibrated to match relevant clinical and/or experimental recordings. In non-fibrotic tissue, membrane kinetics were represented with a human atrial model under chronic AF conditions.[27,28] Conductivity tensor values were calibrated by conducting simulations in a test geometry (4.5 cm × 4.5 cm × 0.5 cm slab, uniform left-to-right fibre orientation) under tachypacing conditions (2 Hz) to obtain longitudinal conduction velocity (CV) of 43.39 cm/s, consistent with CV observed via high-density mapping of induced AF in humans (between 38 and 54 cm/s).[29] When the same conductivity tensor values were used in tachypacing simulations conducted in a wedge model of atrial tissue with realistic fibre orientations and regions of fibrotic remodelling, we observed CV values consistent with the target range [min: 15.18; max: 47.81 cm/s; median (interquartile range): 31.46 (28.38–36.32) cm/s].

In fibrotic tissue, further cell-scale changes were made to represent changes due to remodelling: −50% I_{K1}, −50% I_{CaL}, −40% I_{Na}.[30–32] Moreover, conductivity in fibrotic tissue regions was reduced by 30% (resulting in longitudinal CV of 20 cm/s) to represent changes in extracellular matrix composition and the anisotropy ratio was increased from 5:1 in non-fibrotic to 8:1 to account for the fact that fibrosis slows CV more dramatically in the direction transverse to cardiac fibres.[33,34]

Notably, the cell- and tissue-scale electrophysiological modelling approach used in this article and other recent studies[12–16] is distinct from an early work on AF published by our group, in which fibrotic tissue regions were represented as consisting of coupled myocytes and fibroblasts based on *in vitro* observations.[22–24] We opted to abandon this method in favour of our more recently-developed approach because no evidence has emerged in support of the notion that fibroblasts couple electrically

to myocytes in intact tissue *in vivo*. A systematic comparison of the many possible ways in which fibrotic remodelling can be represented in computational models can be found elsewhere.[35]

Simulations conducted for this study were performed in models with EP_{avg}, as described in the paragraph above and elsewhere.[12–16] However, we compare the results of these simulations to previously-published findings from our analysis from atrial models with ±10% APD or CV (i.e. variable EP—EP_{var}).[14] Complete details regarding those simulations, including the parameter changes used to produce ±10% APD/CV, can be found in that article.[14]

Initiation of atrial fibrillation in post-ablation models

In our previous study,[14] we provided a comprehensive assessment of all AF-perpetuating RDs observed in all 12 patient-specific atrial models, under both EP_{avg} and EP_{var} conditions. These data, which are presented in the original study[14] (see *Figure 3* and Supplementary *Figures S1-S11* of that paper), serve as the starting point for the present study. In all 12 models, we simulated ablation of all EP_{avg} RD trajectories, as shown in *Figure 1*. Virtual ablation lesions consisted of the tissue volumes within 0.35 cm (i.e. the ablation lesion radius for standard irrigated-tip catheters)[7] of each RD trajectory; as in previous work,[13,15,36] the contained tissue volume was modelled as non-conductive.

Then, inducibility of re-entrant arrhythmias in each patient-specific model under EP_{avg} conditions was assessed by applying a clinically relevant rapid electrical pacing sequence[37] from 15 locations evenly distributed in the left and right atria, as in previous studies.[12–16] The outcome of pacing was classified as arrhythmia if the last pacing stimulus was followed by at least 2000 ms of self-sustaining activity. Each induced episode of arrhythmia was then further sub-classified, either as macro-reentry, in cases where uninterrupted propagation was observed around a non-conductive anatomical obstacle (e.g. mitral/tricuspid valve annuli, ostia of pulmonary veins), or as an emergent AF-perpetuating RD sustained by the fibrotic substrate.

In all cases of RD-perpetuated AF, RDs were identified using the previously-described dynamic wavefront tip trajectory approach,[14] which is faster and less sensitive to false positives than the phase singularity-based method we have used previously.[12] Briefly, RD wavefront 'pivot points' were manually identified during the last 1000 ms of each simulation. This ensured that multiple RD rotations were analysed and that transient instability immediately following AF initiation was disregarded. In all cases, RDs persisted for at least two rotations and lasted at >200 ms, which is consistent with clinical definitions for RD persistence.[6,37] Re-entrant driver location was defined as the midpoint between extrema.

To test our mechanistic hypothesis regarding arrhythmia dynamics in post-ablation models, we compared the locations of emergent RDs in EP_{avg} models and pre-ablation RDs in EP_{var} models from our previous study, as illustrated by the schematic in *Figure 2*. To facilitate pair-wise comparison of RD locations, we defined an ablation lesion volume around each RD trajectory, as described above. Inter-RD distance (d) was defined by identifying the shortest path between the boundaries of the two volumes of interest; for overlapping volumes, $d = 0$ by definition.

All electrophysiological simulations were conducted using the CARP software package (Cardiosolv, LLC)[38,39] on a high-performance computing system. Each second of simulated activity required ~30 min of computing time on 24 Intel Xeon CPU cores (2.80 GHz) in parallel.

Statistics

Continuous variables were expressed as mean ± standard deviation and compared using the Wilcoxon signed-rank test (for paired data) or the Mann–Whitney test (unpaired data). Categorical variables were expressed as percentages. All tests were two-tailed; $P < 0.05$ indicated statistical significance.

Results

Post-ablation rapid pacing induced re-entrant arrhythmia in 9 of 12 patient-specific atrial models. In three cases (Patients 9, 11, and 12), the virtual ablation lesion sets (i.e. locations of RDs in pre-ablation simulations conducted under EP_{avg} conditions) shown in *Figure 1* rendered arrhythmia completely non-inducible; in the remaining nine models, at least one episode of AF perpetuated by emergent RD was

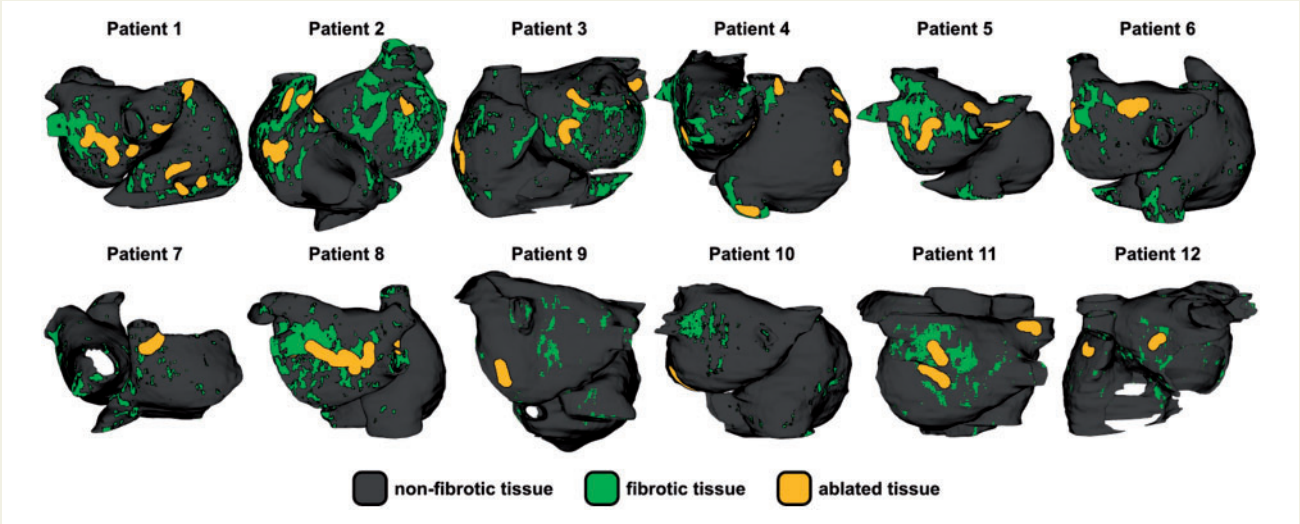

Figure 1 Distribution of fibrotic tissue and locations of ablated RDs in all 12 patient-specific atrial models. Ablated tissue regions correspond to RD trajectories observed under EP_{avg} condition in previous study by Deng *et al.*[14] EP_{avg}, average AF electrophysiology; RD, re-entrant driver.

observed. Data for all 12 cases are presented in *Table 1*. Emergent RDs dynamically localized to between 1 and 4 (1.75 ± 1.35) spatially distinct sites (i.e. with non-overlapping RD trajectories), which was significantly fewer than the number of distinct RD sites in pre-ablation models (4.08 ± 2.27, $P < 0.01$). Notably, for the three models that were completely non-inducible, the number of pre-ablation RD sites was relatively low (range 1–3). Among the nine patient-specific models in which arrhythmia episodes were induced post-ablation, the number of pacing sites that induced each type of arrhythmia was as follows: RD-perpetuated AF, 3.33 ± 1.8 of 15 (range 1–6); macro-reentry around ablation lesion(s), 2.33 ± 1.73 of 15 (range 0–5); and, macro-reentry around anatomical obstacle, 2.77 ± 1.3 of 15 (range 1–5).

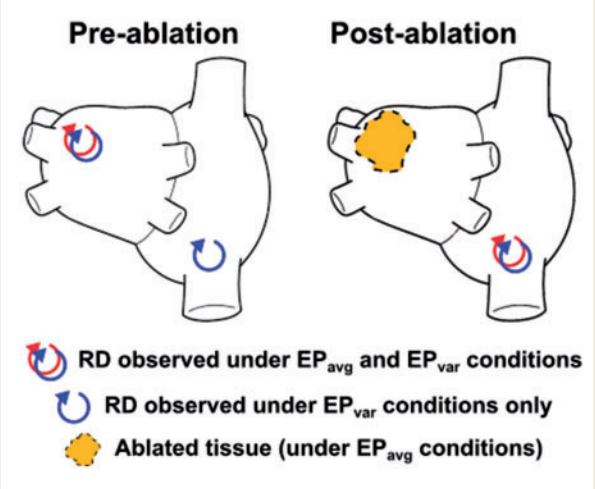

Figure 2 Schematic illustrating the mechanistic hypothesis tested in this study. Sites of pre-ablation RDs for both simulations conducted under both EP_{avg} and EP_{var} conditions were established in a previous study.[14] In some cases, RD sites observed under EP_{var} conditions were never observed in EP_{avg} simulations (left panel). We hypothesized that if virtual ablation was used to destroy the substrate for all EP_{avg} RDs, reapplying the AF induction protocol would result in initiation of emergent RDs (right panel) in locations that were previously only observed under EP_{var} conditions. AF, atrial fibrillation; EP_{avg}, average AF electrophysiology; EP_{var}, variable electrophysiology; RD, re-entrant driver.

Cycle lengths for pre- and post-ablation RDs as well as episodes of post-ablation macro-reentry are presented in *Table 2*. Post-ablation RDs were significantly faster (i.e. shorter cycle length) than pre-ablation RDs (251.9 ± 44 ms vs. 278.6 ± 50.63 ms; $P < 0.05$). In contrast, post-ablation macro-reentry consistently had a longer cycle length than post-ablation RDs, both at the level of individual patient-specific models (i.e. row-by-row comparisons) and overall (293.9 ± 72.49 ms; $P < 0.05$ vs. post-ablation RDs).

Figure 3 presents activation maps corresponding to specific examples in which rapid pacing resulted in macro-reentry around ablation lesion(s). In all four cases, the highlighted re-entrant circuit was the sole driver perpetuating arrhythmic activity for the duration of the simulation after the end of rapid pacing. Interestingly, there was no obvious relationship between the number of ablation lesions (i.e. 'pre-ablation' column in *Table 1*) and the frequency with which rapid pacing led to the initiation of this type of re-entry. For example, in the two patient-specific models with the largest number of ablation lesions ($n = 8$, Patients 1 and 4), only two episodes each were observed.

Figure 4 also presents a series of activation maps, but in this case for induced episodes of RD-perpetuated AF. Each panel shows a paired set of maps: on the left, an RD observed in the pre-ablation model in simulations performed under EP_{var} conditions as part of the previous study by Deng *et al.*[14]; on the right, an emergent RD seen in

Table 1 Dynamics of arrhythmia induced by rapid pacing in all 12 patient-specific atrial models

	Number of distinct RD sites		Number of sites (n/15) from which rapid pacing resulted in each type of arrhythmia		
Patients	**Pre-ablation**	**Post-ablation**	**AF perpetuated by RD**	**Macro-reentry around lesion**	**Macro-reentry around vein**
1	8	2	5	2	3
2	5	3	5	4	3
3	5	4	6	0	1
4	8	2	4	2	1
5	4	3	3	5	5
6	2	2	2	2	2
7	2	3	3	2	3
8	5	1	1	4	3
9	1	0	–	–	–
10	4	1	1	0	4
11	3	0	–	–	–
12	2	0	–	–	–
Summary	4.08 ± 2.27 (n = 12)	1.75 ± 1.35 (n = 12)	3.33 ± 1.8 (n = 9)	2.33 ± 1.73 (n = 9)	2.77 ± 1.3 (n = 9)

Results in the 'pre-ablation' column are from Deng *et al.*[14]
AF, atrial fibrillation; RD, re-entrant driver.

Table 2 Cycle lengths in milliseconds (mean ± SD) for pre- and post-ablation RDs and for post-ablation macro-reentry

Patients	Pre-ablation RD cycle lengths	Post-ablation RD cycle lengths	Post-ablation macro-reentry cycle lengths
1	280.71 ± 54.24	285 ± 35.36	322.5 ± 95.7
2	345 ± 23.18	276.67 ± 58.59	332.5 ± 91.79
3	245.86 ± 23.95	235 ± 33.17	220
4	263.33 ± 30.72	245 ± 21.21	263.33 ± 49.33
5	295.71 ± 69.19	273.33 ± 76.38	290 ± 27.08
6	248.33 ± 28.43	230 ± 14.14	240 ± 40
7	242.5 ± 3.54	230 ± 30	275 ± 17.32
8	305.89 ± 57.42	290	352.5 ± 99.12
9	250	na	na
10	257.07 ± 32.21	200	210
11	276.67 ± 40.41	na	na
12	225 ± 7.07	na	na
Summary	278.6 ± 50.63 ms ($n = 81$)	251.9 ± 44 ms ($n = 21$)	293.9 ± 72.49 ms ($n = 28$)
Differences	$P < 0.05$	$P < 0.05$	

Results in 'pre-ablation RDs' column are from Deng *et al.*[14]
P-values in row labelled 'Differences' are derived from the Mann–Whitney test comparing adjacent columns (i.e. pre-ablation vs. post-ablation RDs and post-ablation RDs vs. post-ablation macro-reentry).
na, no RDs inducible; RD, re-entrant driver; SD, standard deviation.

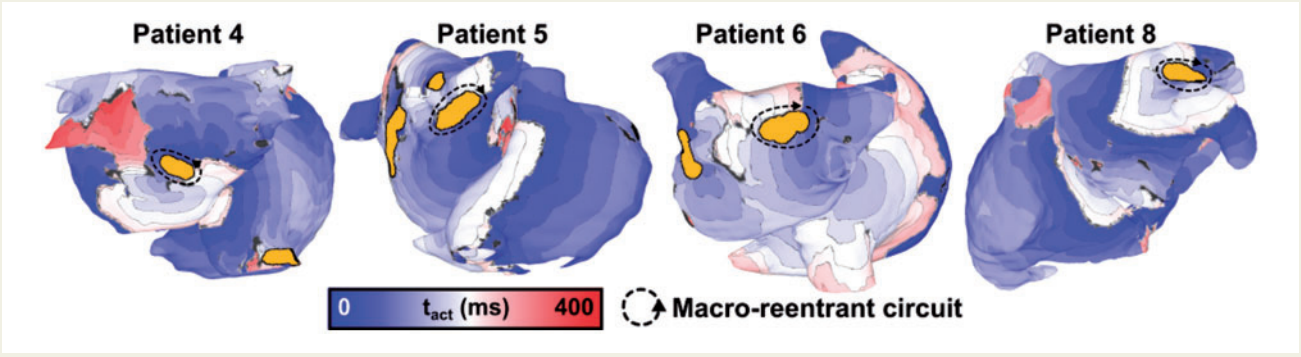

Figure 3 Examples of macro-reentrant arrhythmia anchored to an ablation lesion. Each case shows activation times rendered on the atrial model. Locations of macro-reentrant circuits are as follows: postero-inferior LA (Patient 4); carina between right pulmonary veins (Patient 5); posterior LA (Patient 6); and anterior LA, between LA appendage and left superior pulmonary vein (Patient 8). Isochrone lines are 25 ms apart. Regions of grey tissue did not undergo an activation during the interval shown. LA, left atrium; t_{act}, local activation time.

the post-ablation model under EP_{avg} conditions. In all cases, the arrhythmia morphology seen in the right-hand panel was never observed in EP_{avg} simulations conducted pre-ablation. For the example shown in Patient 1 (*Figure 4A*), the distance between the RD trajectory and the nearest region of ablated tissue in the EP_{avg} model was 0.48 cm; for the other three examples shown, this value was 0.096 cm (Patient 2; *Figure 4B*), 0.61 cm (Patient 7; *Figure 4C*), and 2.8 cm (Patient 10; *Figure 4D*). Conduction velocity values were computed at all non-ablated points in both atrial chambers for all four episodes of post-ablation RD-perpetuated AF shown in *Figure 4*; measured CV values were within the range of values derived from clinical mapping of patient hearts with induced AF[29] (*4A*: min. 10.59 cm/s, max. 47.31 cm/s, mean 31.72 ± 7.99 cm/s; *4B*: min. 10.51 cm/s, max. 46.44 cm/s, mean 28.63 ± 8.34 cm/s; *4C*: min. 10.22 cm/s, max. 45.06 cm/s, mean 30.05 ± 6.89 cm/s; *4D*: min. 11.96 cm/s, max. 42.44 cm/s, mean 26.89 ± 6.75 cm/s).

For all four cases shown here, the RD location in the post-ablation EP_{avg} model was an excellent match for the RD site observed in the pre-ablation EP_{var} model ($d = 0$; i.e. overlapping trajectories). This supports the mechanistic hypothesis articulated in the Introduction section and illustrated schematically in *Figure 2*. Interestingly, for one of the examples (Patients 7; *Figure 4C*), the RDs observed in the EP_{var} and EP_{avg} cases had opposite chirality (i.e. clockwise vs. counter-clockwise), suggesting that the properties of the underlying fibrotic

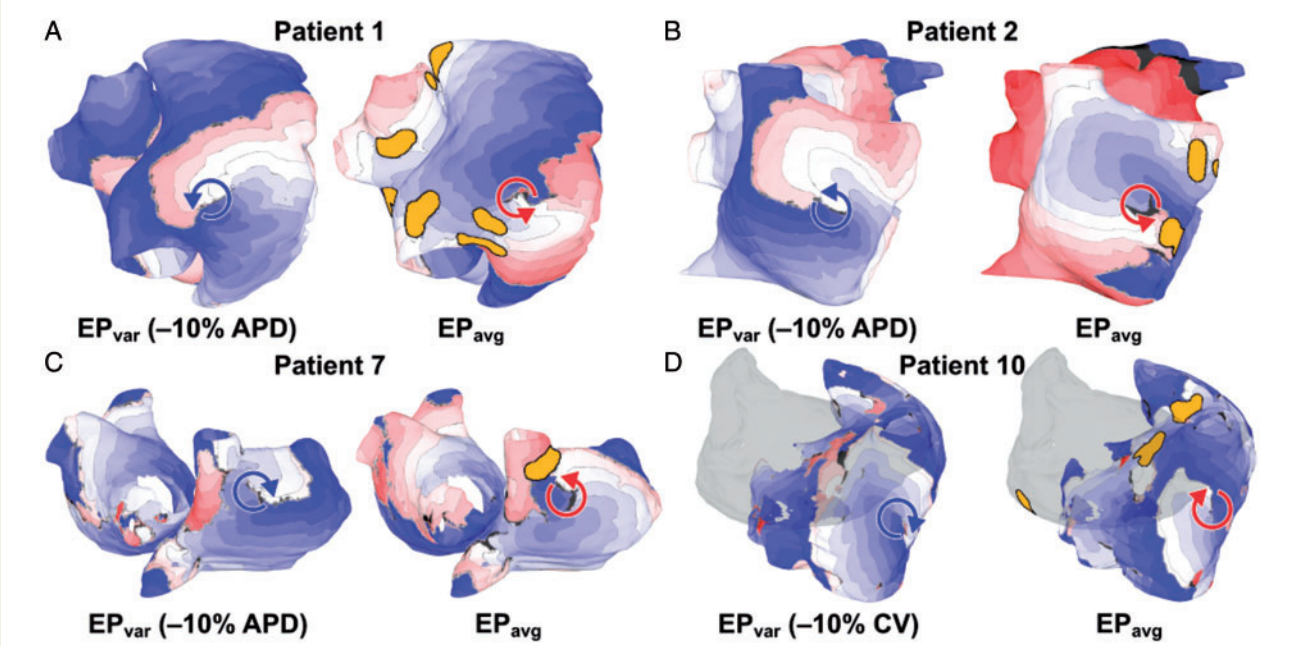

Figure 4 Examples of RD-perpetuated AF in pre- and post-ablation atrial models. Each panel shows a side-by-side comparison of an RD that was induced in the pre-ablation model under one of the EP_{var} conditions (left) and an RD in the same location that was induced in the post-ablation model under EP_{avg} conditions (right). In all four cases shown, the pre- and post-ablation RD trajectories overlap ($d = 0$). (*A*) RDs located in infero-lateral RA, near IVC. (*B*) RDs located on lateral RA. (*C*) RDs located on posterior RA, near SVC. Note difference in chirality (left: clockwise, right: counter-clockwise). (*D*) RDs located between IVC and SVC. LA is shown in silhouette for ease of visualization. Same colour scale as *Figure 3*. AF, atrial fibrillation; EP_{avg}, average AF electrophysiology; EP_{var}, variable electrophysiology; LA/RA, left/right atrium; RD, re-entrant driver; SVC/IVC, superior/inferior vena cava.

substrate strongly favour RD initiation and perpetuation regardless of exact nature and timing of the excitation wavefronts that enter that region during rapid pacing. Notably, while the examples shown here were all RDs located in the right atria, overlapping RDs were also seen in the LA; likewise, while 3/4 examples shown here involve results from −10% APD simulations, overlapping RDs were found for all four EP_{var} conditions (±10% APD/CV).

Comprehensive summary data for all 21 emergent RDs observed in all post-ablation simulations are presented in joint schematic and tabular form in *Figure 5* and *Table 3*, respectively. In *Figure 5*, each emergent RD location in the atrial model corresponding to Patient *X* is marked by a purple or yellow circle containing a number *Y*; detailed information about each RD can be found by referring to the row of *Table 3* with *X* in column 1 and *Y* in column 2. For 13/21 (62%) emergent RDs observed in post-ablation simulations conducted under EP_{avg} conditions, the trajectory overlapped spatially (i.e. $d = 0$, as described in Methods section) with an RD that was observed pre-ablation in the same atrial model for simulations conducted under at least one EP_{var} condition, as described by Deng *et al.*[14]; these cases are indicated by the purple circles. For the remaining 8/21 emergent RDs (yellow circles), there was no overlapping trajectory from EP_{var} simulations (i.e. $d > 0$); however, 2/8 cases were very close to being classified as overlapping ($d \leq 0.1$ cm) and the overall distance between non-overlapping emergent RD targets and the nearest RDs in pre-ablation EP_{var} simulations was relatively small ($d = 1.44 \pm 1.29$ cm). Interestingly, 5/8 non-overlapping emergent RDs were located in completely distinct locations where RDs were not seen pre-ablation regardless of the electrophysiological condition used in the model (i.e. EP_{avg} or EP_{var}). Consistent with previous computational and clinical studies by our group, the organizing centres of all observed emergent RDs localized to boundaries between fibrotic and non-fibrotic tissue regions.[12,15,16,35,40]

Discussion

In this study, we used computational models reconstructed from LGE-MRI scans of the fibrotic atria of individuals with PsAF to assess the dynamics of arrhythmia following virtual ablation of an initial set of RDs. To the best of our knowledge, this was the first attempt to characterize this behaviour in realistic organ-scale models including detailed representations of atrial geometry and patient-specific patterns of structural remodelling. We showed that: (i) a majority of emergent RDs (15/21, 71.4%) that manifested in post-ablation simulations conducted under EP_{avg} conditions dynamically localized to the same atrial regions (within <0.1 cm) where RDs were previously found under EP_{var} conditions in pre-ablation models; (ii) emergent RDs occurred in regions at boundaries between fibrotic and non-fibrotic atrial tissue; and (iii) in a majority of post-ablation models in which virtual ablation did not render arrhythmia non-inducible (7/9, 77.8%), at least one episode of macro-reentry around ablation lesion(s) was observed.

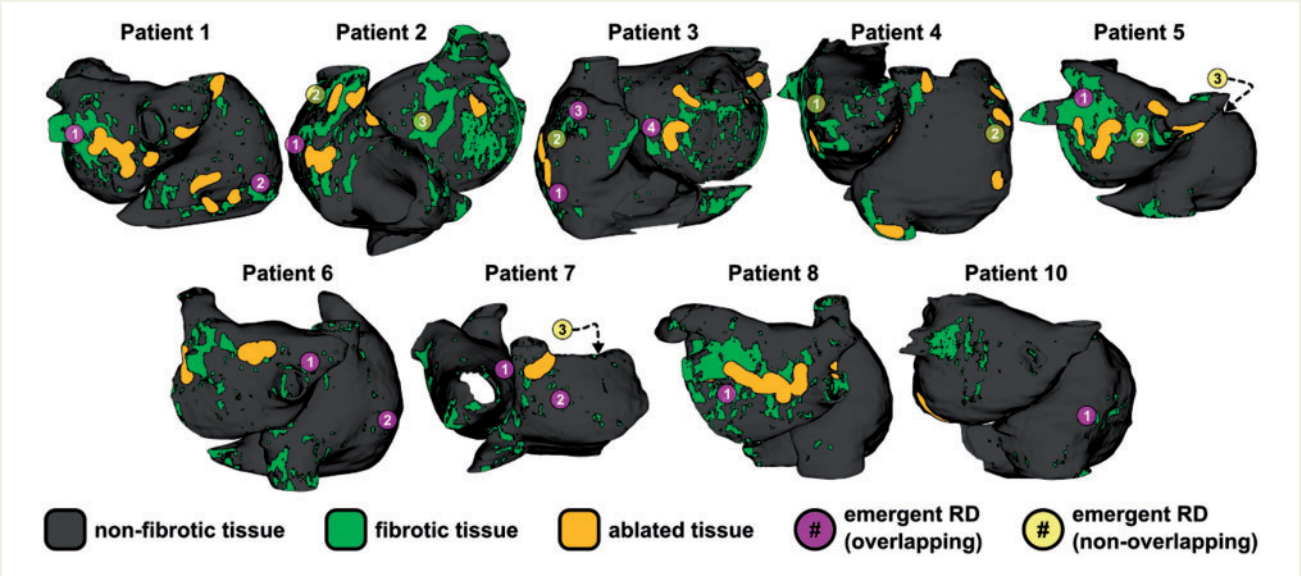

Figure 5 Locations of all 21 emergent RDs simulations conducted post-ablation in models under EP_{avg} conditions. In 3/12 patients, no RDs were induced (Patients 9, 11, and 12). Purple circles indicate emergent RDs that overlapped with pre-ablation RDs observed in simulations conducted under EP_{var} conditions (13/12); yellow circles indicate emergent RDs that did not overlap (8/21). See *Table 3* for detailed information, including distance (*d*) values corresponding to all yellow points. Some RD sites shown correspond to activation maps shown in EP_{avg} panels of *Figure 4*: Patient 1, RD2 = *4A*; Patient 2, RD1 = *4B*; Patient 7, RD2 = *4C*; Patient 10, RD1 = *4D*. EP_{avg}, average AF electrophysiology; EP_{var}, variable electrophysiology; RD, re-entrant driver.

The results presented here expand our growing understanding that each PsAF patient's unique pattern of fibrotic remodelling needs to be considered when planning ablation procedures that aim to modify the substrate and thus abolish its pro-arrhythmic properties. Previous computational and clinical work from our group has shown that pre-ablation RDs localize to a specific subset of boundaries between fibrotic and non-fibrotic myocardium[12,15,16,35,40] and we have thus speculated that computational simulations could be used to generate a comprehensive list of ablation targets for each individual.[18] However, we have also shown that the feasibility of such an approach might be limited by the fact that RD localization dynamics in pre-ablation atrial models reconstructed with non-invasive measures alone (i.e. conducted under EP_{avg} conditions) could be sensitive to variations in APD and CV.[14]

In this study, we show that the level of uncertainty in our models' ability to predict patient-specific ablation targets can be substantially mitigated by running additional simulations that include virtual ablation of RDs. Specifically, our findings reveal that many potential RD-harbouring locations, previously observed only in simulations conducted under EP_{var} conditions, can be unmasked by re-applying the same AF-initiating rapid pacing protocol to the post-ablation model under EP_{avg} conditions (13/21 overlapped; 15/21, $d \leq 0.1$ cm). This strongly supports our mechanistic hypothesis and suggests that any efforts towards simulation-based planning of clinical catheter ablation procedures must include an iterative process of RD identification, virtual ablation, and AF re-induction to locate emergent RDs.

Interestingly, five emergent RDs were observed in areas that were completely distinct from any RDs observed in any pre-ablation simulations, regardless of whether they were conducted under EP_{avg} or EP_{var} conditions. This suggests that some regions within the fibrotic substrate, despite having the intrinsic capacity to sustain RDs, may be completely latent in pre-ablation atrial models, even when APD/CV values are changed to represent inter-patient variability in EP properties. It follows that it may also be impossible to map RD activity in some atrial regions prior to clinical ablation, which suggests a potential explanation for why efforts to improve PsAF ablation outcomes by targeting mapped RDs have yet to yield satisfactory results. This lends further support to the iterative induce/ablate/re-induce concept outlined above. If properly validated, this approach could potentially be used prior to each PsAF ablation procedure to generate a comprehensive list of potential RD targets in each individual.

Results in this study are consistent with the findings of a simulation study of ablation targeting RDs in two-dimensional atrial sheets,[10] and in particular, that ablating the RD trajectory alone creates a new substrate for the initiation and perpetuation of macro-reentry around the lesion. This suggests that when RD sites are identified (by FIRM, ECGI, analysis of patient-specific simulations, or any other means) and targeted for ablation, additional linear lesions must also be created between the RD region and a non-conductive barrier (e.g. mitral or tricuspid valve annuli, sleeves of pulmonary veins, existing PVI lines). This is a crucial step to eliminate the possibility of post-ablation atrial tachycardia or flutter, which is difficult to treat and has deleterious consequences similar to AF.[41–43]

Limitations

Our findings must be interpreted in the context of a few noteworthy limitations. First, our approach for parameterizing conductivity tensor

Table 3 Detailed information about all 21 emergent RDs shown in *Figure 5*

Patients	RD# in *Figure 5*	Qualitative description of emergent RD location	Distance to nearest EP_{var} site (cm)	Distance to nearest EP_{avg} RD ablation (cm)
1	1	Posterior LA, near LIPV	–	0.709
	2[a]	Infero-lateral RA	–	0.484
2	1[a]	Lateral RA	–	0.096
	2[b]	Near SVC	2.86	1.71
	3[b]	Anterior LA	1.56	2.47
3	1	Infero-lateral RA	–	0.700
	2	Lateral RA	0.138	–
	3	Base of RAA	–	0.818
	4	Anterior LA, near mitral valve annulus	–	–
4	1[b]	Posterior LA, near RIPV	2.57	1.10
	2	Lateral RA	0.0688	–
5	1	Posterior LA, near LSPV	–	–
	2	Posterior LA, near RIPV	0.699	–
	3[b]	Anterior RA, near RAA (not visible in *Figure 5*)	3.4	5.33
6	1	Carina between RSPV and RIPV	–	–
	2	Lateral RA	–	5.75
7	1	Anterior LA, near RSPV	–	0.733
	2[a]	Lateral RA	–	0.606
	3[b]	Anterior RA, near RAA (not visible in *Figure 5*)	1.38	0.973
8	1	Posterior LA, inferior to LIPV	–	0.0370
10	1[a]	Posterior RA, superior to IVC	–	2.76

Distances to EP_{var} sites are only provided for emergent RDs that did not correspond to an RD observed in the same location in pre-ablation simulations under EP_{var} conditions, as described by Deng *et al.*[14]

EP_{avg}, average AF electrophysiology; EP_{var}, variable electrophysiology; IVC, inferior vena cava; LA, left atrium; LIPV, left inferior pulmonary vein; LSPV, left superior pulmonary vein; RA, right atrium; RAA, right atrial appendage; RD, re-entrant driver; RIPV, right inferior pulmonary vein; RSPV, right superior pulmonary vein; SVC superior vena cava.

[a]RDs for which activation maps are shown in *Figure 4*.

[b]Emergent RDs that were completely distinct from any RDs observed in any pre-ablation simulations, regardless of whether they were conducted under either EP_{avg} or EP_{var} conditions.

parameters used simulations of non-re-entrant wave propagation in a rapidly paced slab tissue model to achieve CV values consistent with those measured during AF in humans (38–54 cm/s).[29] The same study reported higher CV values for sinus rhythm (73 cm/s) and paced activation (68 cm/s). We used this approach for conductivity parameterization because models with different intrinsic CVs would necessitate different rapid pacing sequences in order to induce AF, so it would be extremely computationally burdensome to perform the necessary calibration experiments to use CV during AF as the target parameter. Despite this limitation, measured values of CV during simulated AF episodes are within the physiological range ($\sim 30 \pm 8$ cm/s), suggesting that our representation of tissue-scale electrophysiological properties is reasonable.

Because effective CV observed during our simulated AF episodes is somewhat lower than what has been measured clinically ($\sim$38 to 54 cm/s),[29] cardiac wavelength (i.e. CV $\times$ APD) is also reduced, which leads to increased likelihood of RD initiation. Indeed, in our earlier paper,[14] we observed a trend towards lower RD inducibility in simulations with +10% CV compared with those with −10% CV (3.5 ± 3.849 vs. 5.083 ± 3.423; $P = 0.0781$). Lower CV would also be expected to increase the likelihood of spiral wave breakup and degeneration into more chaotic behaviour; despite this fact, we almost never observe concomitant RDs in our simulations. We attribute this to the strong propensity for RD anchoring that exists at some boundaries between fibrotic and non-fibrotic tissue, which has been characterized and discussed at length in our previous studies of AF.[12,15,16,40] Only particular boundary regions of fibrotic remodelling anchor persistent RDs, and it is these persistent RDs (and not any transient ones) that drive the activity in the atria. Importantly, these are the RDs that are the targets of ablation in PsAF in atria with fibrotic remodelling.

We found that post-ablation RD cycle lengths were significantly shorter than those observed pre-ablation. This is an intriguing observation, since acute AF cycle length prolongation in the clinical context implies a higher degree of organization and, as such, is classified as a positive response to ablation.[6] However, as we discussed in our previous study,[14] RD cycle lengths from our simulations should not be compared directly to clinical measurements of AF cycle length, since the latter measurements integrate effects from many different underlying factors (RDs, ectopic foci, sinus beats, etc.), while the former are derived from RDs that persist in the absence of other factors.

Finally, several studies recent studies have reported that other structural factors, such as heterogeneity of atrial wall thickness[44] and the complex micro-structure of the atrial endocardium[45] can

influence the dynamics of AF perpetuation, including re-entrant source localization. In contrast, this study is concerned specifically with the relationship between the macroscopic patient-specific distribution of fibrotic tissue and the emergent dynamics of RD localization pre- and post-ablation. Although our computational models include a realistic representation of the complex transmural pattern of fibre orientations, they are based on an image reconstruction methodology that assumes a uniform atrial wall thickness. Moreover, the resolution of the clinical scans from which models are reconstructed is insufficient to resolve sub-millimetre structural features on the endocardium. As such, we emphasize that the mechanisms revealed by our analysis may in reality interact with other potential factors to give rise to the complex behaviour of AF-perpetuating RDs and sources of triggered excitation.

Conclusion

Following virtual ablation of RDs in computational models of the atria, new episodes of arrhythmia can be perpetuated by emergent RDs or by macro-reentrant circuits that form around lesions. As such, efforts to custom-tailor clinical PsAF ablation procedures based on analysis of simulations conducted in patient-specific models reconstructed from LGE-MRI must both include steps to identify post-ablation emergent RDs and linear lesions between ablated RD regions and non-conductive barriers to prevent macro-reentry.

Funding

This work was supported by American Heart Association 16-SDG-30440006 (to P.M.B.) and by NIH DP1-HL123271 (to N.A.T.).

Conflict of interest: none declared.

References

1. Colilla S, Crow A, Petkun W, Singer DE, Simon T, Liu X. Estimates of current and future incidence and prevalence of atrial fibrillation in the U.S. adult population. *Am J Cardiol* 2013;**112**:1142–7.
2. Nattel S, Guasch E, Savelieva I, Cosio FG, Valverde I, Halperin JL *et al.* Early management of atrial fibrillation to prevent cardiovascular complications. *Eur Heart J* 2014;**35**:1448–56.
3. Calkins H, Hindricks G, Cappato R, Kim YH, Saad EB, Aguinaga L *et al.* HRS/EHRA/ECAS/APHRS/SOLAECE expert consensus statement on catheter and surgical ablation of atrial fibrillation. *Europace* 2018;**20**:e1–160.
4. Verma A, Jiang CY, Betts TR, Chen J, Deisenhofer I, Mantovan R *et al.* Approaches to catheter ablation for persistent atrial fibrillation. *N Engl J Med* 2015;**372**:1812–22.
5. Mandapati R, Skanes A, Chen J, Berenfeld O, Jalife J. Stable microreentrant sources as a mechanism of atrial fibrillation in the isolated sheep heart. *Circulation* 2000;**101**:194–9.
6. Haissaguerre M, Hocini M, Denis A, Shah AJ, Komatsu Y, Yamashita S *et al.* Driver domains in persistent atrial fibrillation. *Circulation* 2014;**130**:530–8.
7. Narayan SM, Krummen DE, Shivkumar K, Clopton P, Rappel WJ, Miller JM. Treatment of atrial fibrillation by the ablation of localized sources: CONFIRM (Conventional Ablation for Atrial Fibrillation With or Without Focal Impulse and Rotor Modulation) trial. *J Am Coll Cardiol* 2012;**60**:628–36.
8. Narayan SM, Baykaner T, Clopton P, Schricker A, Lalani GG, Krummen DE *et al.* Ablation of rotor and focal sources reduces late recurrence of atrial fibrillation compared with trigger ablation alone: extended follow-up of the CONFIRM trial (Conventional Ablation for Atrial Fibrillation With or Without Focal Impulse and Rotor Modulation). *J Am Coll Cardiol* 2014;**63**:1761–8.
9. Mohanty S, Mohanty P, Trivedi C, Gianni C, Della Rocca DG, Di Biase L *et al.* Long-term outcome of pulmonary vein isolation with and without focal impulse and rotor modulation mapping: insights from a meta-analysis. *Circ Arrhythm Electrophysiol* 2018;**11**:e005789.
10. Rappel WJ, Zaman JA, Narayan SM. Mechanisms for the termination of atrial fibrillation by localized ablation: computational and clinical studies. *Circ Arrhythm Electrophysiol* 2015;**8**:1325–33.
11. Trayanova NA. Mathematical approaches to understanding and imaging atrial fibrillation: significance for mechanisms and management. *Circ Res* 2014;**114**:1516–31.
12. Zahid S, Cochet H, Boyle PM, Schwarz EL, Whyte KN, Vigmond EJ *et al.* Patient-derived models link re-entrant driver localization in atrial fibrillation to fibrosis spatial pattern. *Cardiovasc Res* 2016;**110**:443–54.
13. Zahid S, Whyte KN, Schwarz EL, Blake RC, Boyle PM, Chrispin J *et al.* Feasibility of using patient-specific models and the "minimum cut" algorithm to predict optimal ablation targets for left atrial flutter. *Heart Rhythm* 2016;**13**:1687–98.
14. Deng D, Murphy MJ, Hakim JB, Franceschi WH, Zahid S, Pashakhanloo F *et al.* Sensitivity of reentrant driver localization to electrophysiological parameter variability in image-based computational models of persistent atrial fibrillation sustained by a fibrotic substrate. *Chaos* 2017;**27**:093932.
15. Boyle PM, Hakim JB, Zahid S, Franceschi WH, Murphy MJ, Vigmond EJ *et al.* Comparing reentrant drivers predicted by image-based computational modeling and mapped by electrocardiographic imaging in persistent atrial fibrillation. *Front Physiol* 2018;**9**:414.
16. Boyle PM, Hakim JB, Zahid S, Franceschi WH, Murphy MJ, Prakosa A *et al.* The fibrotic substrate in persistent atrial fibrillation patients: comparison between predictions from computational modeling and measurements from focal impulse and rotor mapping. *Front Physiol* 2018;**9**:1151.
17. Boyle PM, Zahid S, Trayanova NA. Towards personalized computational modelling of the fibrotic substrate for atrial arrhythmia. *Europace* 2016;**18**:iv136–45.
18. Boyle PM, Zahid S, Trayanova NA. Using personalized computer models to custom-tailor ablation procedures for atrial fibrillation patients: are we there yet? *Expert Rev Cardiovasc Ther* 2017;**15**:339–41.
19. Andrade J, Khairy P, Dobrev D, Nattel S. The clinical profile and pathophysiology of atrial fibrillation: relationships among clinical features, epidemiology, and mechanisms. *Circ Res* 2014;**114**:1453–68.
20. Khurram IM, Beinart R, Zipunnikov V, Dewire J, Yarmohammadi H, Sasaki T *et al.* Magnetic resonance image intensity ratio, a normalized measure to enable interpatient comparability of left atrial fibrosis. *Heart Rhythm* 2014;**11**:85–92.
21. Vadakkumpadan F, Arevalo H, Ceritoglu C, Miller M, Trayanova N. Image-based estimation of ventricular fiber orientations for personalized modeling of cardiac electrophysiology. *IEEE Trans Med Imaging* 2012;**31**:1051–60.
22. McDowell KS, Vadakkumpadan F, Blake R, Blauer J, Plank G, MacLeod RS *et al.* Methodology for patient-specific modeling of atrial fibrosis as a substrate for atrial fibrillation. *J Electrocardiol* 2012;**45**:640–5.
23. McDowell KS, Vadakkumpadan F, Blake R, Blauer J, Plank G, Macleod RS *et al.* Mechanistic inquiry into the role of tissue remodeling in fibrotic lesions in human atrial fibrillation. *Biophys J* 2013;**104**:2764–73.
24. McDowell KS, Zahid S, Vadakkumpadan F, Blauer J, MacLeod RS, Trayanova NA. Virtual electrophysiological study of atrial fibrillation in fibrotic remodeling. *PLoS One* 2015;**10**:e0117110.
25. Pashakhanloo F, Herzka DA, Ashikaga H, Mori S, Gai N, Bluemke DA *et al.* Myofiber architecture of the human atria as revealed by submillimeter diffusion tensor imaging. *Circ Arrhythm Electrophysiol* 2016;**9**:e004133.
26. Fastl TE, Tobon-Gomez C, Crozier A, Whitaker J, Rajani R, McCarthy KP *et al.* Personalized computational modeling of left atrial geometry and transmural myofiber architecture. *Med Image Anal* 2018;**47**:180–90.
27. Courtemanche M, Ramirez RJ, Nattel S. Ionic mechanisms underlying human atrial action potential properties: insights from a mathematical model. *Am J Physiol* 1998;**275**:H301–21.
28. Krummen DE, Bayer JD, Ho J, Ho G, Smetak MR, Clopton P *et al.* Mechanisms of human atrial fibrillation initiation: clinical and computational studies of repolarization restitution and activation latency. *Circ Arrhythm Electrophysiol* 2012;**5**:1149–59.
29. Konings KT, Kirchhof CJ, Smeets JR, Wellens HJ, Penn OC, Allessie MA. High-density mapping of electrically induced atrial fibrillation in humans. *Circulation* 1994;**89**:1665–80.
30. Nattel S, Burstein B, Dobrev D. Atrial remodeling and atrial fibrillation: mechanisms and implications. *Circ Arrhythm Electrophysiol* 2008;**1**:62–73.
31. Corradi D, Callegari S, Maestri R, Benussi S, Alfieri O. Structural remodeling in atrial fibrillation. *Nat Clin Pract Cardiovasc Med* 2008;**5**:782–96.
32. Kakkar R, Lee RT. Intramyocardial fibroblast myocyte communication. *Circ Res* 2010;**106**:47–57.
33. Li D, Fareh S, Leung TK, Nattel S. Promotion of atrial fibrillation by heart failure in dogs: atrial remodeling of a different sort. *Circulation* 1999;**100**:87–95.

34. Burstein B, Comtois P, Michael G, Nishida K, Villeneuve L, Yeh YH *et al*. Changes in connexin expression and the atrial fibrillation substrate in congestive heart failure. *Circ Res* 2009;**105**:1213–22.
35. Roney CH, Bayer JD, Zahid S, Meo M, Boyle PM, Trayanova NA *et al*. Modelling methodology of atrial fibrosis affects rotor dynamics and electrograms. *Europace* 2016;**18**:(suppl 4) iv146–55.
36. Arevalo HJ, Vadakkumpadan F, Guallar E, Jebb A, Malamas P, Wu KC *et al*. Arrhythmia risk stratification of patients after myocardial infarction using personalized heart models. *Nat Commun* 2016;**7**:11437.
37. Narayan SM, Krummen DE, Rappel WJ. Clinical mapping approach to diagnose electrical rotors and focal impulse sources for human atrial fibrillation. *J Cardiovasc Electrophysiol* 2012;**23**:447–54.
38. Vigmond EJ, Aguel F, Trayanova NA. Computational techniques for solving the bidomain equations in three dimensions. *IEEE Trans Biomed Eng* 2002;**49**:1260–9.
39. Vigmond EJ, Hughes M, Plank G, Leon LJ. Computational tools for modeling electrical activity in cardiac tissue. *J Electrocardiol* 2003;**36**:69–74.
40. Cochet H, Dubois R, Yamashita S, Al Jefairi N, Berte B, Sellal JM *et al*. Relationship between fibrosis detected on late gadolinium-enhanced cardiac magnetic resonance and re-entrant activity assessed with electrocardiographic imaging in human persistent atrial fibrillation. *JACC Clin Electrophysiol* 2018;**4**:17–29.
41. Gerstenfeld EP, Callans DJ, Dixit S, Russo AM, Nayak H, Lin D *et al*. Mechanisms of organized left atrial tachycardias occurring after pulmonary vein isolation. *Circulation* 2004;**110**:1351–7.
42. Daoud EG, Weiss R, Augostini R, Hummel JD, Kalbfleisch SJ, Van Deren JM *et al*. Proarrhythmia of circumferential left atrial lesions for management of atrial fibrillation. *J Cardiovasc Electrophysiol* 2006;**17**:157–65.
43. Weerasooriya R, Jais P, Wright M, Matsuo S, Knecht S, Nault I *et al*. Catheter ablation of atrial tachycardia following atrial fibrillation ablation. *J Cardiovasc Electrophysiol* 2009;**20**:833–8.
44. Yamazaki M, Mironov S, Taravant C, Brec J, Vaquero LM, Bandaru K *et al*. Heterogeneous atrial wall thickness and stretch promote scroll waves anchoring during atrial fibrillation. *Cardiovasc Res* 2012;**94**:48–57.
45. Hansen BJ, Zhao J, Csepe TA, Moore BT, Li N, Jayne LA *et al*. Atrial fibrillation driven by micro-anatomic intramural re-entry revealed by simultaneous sub-epicardial and sub-endocardial optical mapping in explanted human hearts. *Eur Heart J* 2015;**36**:2390–401.